

Los Alamos National Laboratory is operated by the University of California for the United States Department of Energy under contract W-7405-ENG-36

TITLE FINAL AMPLIFIER DESIGN AND MERCURY

AUTHOR(S) Evan A. Rose, CLS-5
David E. Hanson, T-12

SUBMITTED TO Presentation was made 12 December 1991 at the International Conference on Lasers '91. LA-UR-91-3914, San Diego, CA
This paper is intended for proceedings of that meeting.

DISCLAIMER

This report was prepared as an account of work sponsored by an agency of the United States Government. Neither the United States Government nor any agency thereof, nor any of their employees, makes any warranty, express or implied, or assumes any legal liability or responsibility for the accuracy, completeness, or usefulness of any information, apparatus, product, or process disclosed, or represents that its use would not infringe privately owned rights. Reference herein to any specific commercial product, process, or service by trade name, trademark, manufacturer, or otherwise does not necessarily constitute or imply its endorsement, recommendation, or favoring by the United States Government or any agency thereof. The views and opinions of authors expressed herein do not necessarily state or reflect those of the United States Government or any agency thereof.

By accepting this report, the publisher certifies that the U.S. Government retains a non-exclusive, royalty-free license to publish or reproduce the published form of this report and to allow others to do so for U.S. Government purposes.

This report is published at the publisher's expense. It is published by the publisher as work performed under the auspices of the U.S. Department of Energy.

MASTER

DISTRIBUTION OF THIS DOCUMENT IS UNLIMITED

Los Alamos Los Alamos National Laboratory
Los Alamos, New Mexico 87545

FINAL AMPLIFIER DESIGN AND MERCURY

Evan Rose and David Hanson

University of California, Los Alamos National Laboratory
P. O. Box 1663, Los Alamos, New Mexico 87545

Abstract

The final amplifier for the Mercury KrF excimer facility is being designed. The design exercise involves extensive modeling to predict amplifier performance. Models of the pulsed-power system, including a Child-Langmuir diode with closure, electron-beam energy deposition, KrF laser kinetics, amplified spontaneous emission (ASE), and time-dependent laser extraction in the presence of ASE are presented as a design package. The design exercise indicates that the energy objective of Phase I - 100 joules - will be met.

Introduction

The Mercury KrF excimer laser facility is part of the national inertial confinement fusion (ICF) program. It is the successor to the Aurora facility¹. An overview of the Mercury facility is given in the paper "Mercury KrF ICF Laser/Design and Goals, presented at this conference.

The Mercury facility is designed to meet a set of parameters related to experiments in support of the ICF program. A primary objective of Mercury is to provide a highly reliable laser, obtained at minimal cost. Thus the Mercury facility uses the same building and much of the equipment of Aurora. The first and fourth electron-beam pumped amplifiers from Aurora will be modified to provide two amplifiers for Mercury, Phase I. The final amplifier will be operated at reduced stress to improve reliability.

Phase I has a goal of 100 joules in twenty-four 200-ps pulses. It will demonstrate reliable operation and achieve critical system performance parameters. A kilojoule system (Phase II) is planned after the successful demonstration of Phase I.

Amplifier Modifications

An upgrade of the first amplifier is planned. This amplifier has a 12-cm x 12-cm aperture and a 1-m length, pumped single-sided. The diode foil will be moved 5 cm closer to the extracted volume and a guide magnetic field will be applied. These changes will increase the pumping of the extracted laser volume and provide higher energy pulses to the final amplifier.

The fourth Aurora amplifier had a 100-cm x 100-cm aperture and a 2-m length, pumped double-sided. This amplifier produced 1.3 kJ on target² (36 out of 96 beams) during the Aurora project and produced 10.7 kJ in 650 ns as an unstable resonator. The aperture will be reduced to 30-cm x 40-cm through modification of a surplus laser chamber from one of the eliminated Aurora amplifiers. The diode emitter height will be reduced from 1 m to 35 cm, and pumping will be single-sided. The pulse-forming lines will be reduced in length by one quarter, from 10.8 m (640 ns) to 8.0 m (475 ns). Electron energy will be reduced from 700 kV to 550 kV. These changes will reduce electrical stress and parts count, leading to higher reliability at minimal cost.

System performance will also be enhanced by reducing the electron drift length in the diode, increasing the transparency of the foil-support structure (hibachi), and improving the laser-gas optical quality through a gas recirculation system.

Laser modeling was performed over a parameter range. The specific pump power for the first amplifier was derived from previous experimental results. Pulsed-power modeling was performed for the modified final amplifier and the results matched with the laser modeling to predict energy delivered to target.

Figure 1 shows the diode and laser regions of the modified final amplifier.

Pulsed Power Model

The circuit model for the final amplifier was modified from an Aurora Large Aperture Module (LAM) model, which produced good agreement with experimental pulsed-power parameters. The model was run with the MicroCAP II program from Spectrum Software. Modifications from the LAM model include 1) reduction of the length of the pulse-forming lines from 10.8 m to 8.0 m, 2) reduction of the cathode area from 2 m² to 0.7 m², 3) reduction of the A-K gap from 7.5 cm to 5.0 cm, and 4) re-optimization of the output-switch closing time. The load was modeled as a Child-Langmuir diode with a 3-cm/ μ s closure rate.

The circuit model is shown in Figure 2. Diode performance is shown in Figure 3. The effect of diode closure is to reduce the voltage and increase the current with time. Delivered power, however, is relatively constant.

Not all of the current produced in the diode arrives at the foil. Diode transport and hibachi losses reduce the current. 40% transmission was measured on the PA amplifier in the Aurora facility. That amplifier had a 20-cm x 290-cm cathode emitter with 94% geometric hibachi transparency. 30% transmission was measured on the LAM amplifier, which had a 1-m x 2-m emitter with 82% geometric transparency. The Mercury final amplifier is expected to perform like the Aurora PA, at 40% transmission.

The low observed hibachi transmissions are not understood at present. Modeling with the ISIS code predicts transmissions close to geometrical with magnetic guide fields and open hibachi structures³ as was the case for the Aurora PA. Improved transmission efficiencies may be possible.

Laser Models

Electron-beam Energy Deposition

The spatial power deposition in the laser medium due to the electron beam is calculated using either a one- or three-dimensional (Cartesian) Monte-Carlo electron scattering model⁴. Individual electron trajectories are tracked from the diode side of the foil, through the laser gas, until electrons are either absorbed by a wall or fall below a few keV. A shielded Coulomb form of the scattering cross section is used with a shielding angle specified by Moliere's formula. To specify the energy loss, the straggling distribution follows Landau's theory, with the mean loss rate normalized to Bethe's formula. If the gas mix, pressure, foil, and incident electron energy are specified, this model relates the specific pump power at any point in the amplifier to the current density at the foil.

For the laser dimensions and aspect ratios considered here, it was found from comparisons with the 3-D model that the 1-D model provided adequate accuracy. To control computer costs, the 1-D model was used exclusively.

Figure 4 shows the electron-beam energy-deposition profile for 550-kV electrons.

KrF Laser Kinetics

Initial Partitioning of e-Beam Energy Model We use a Monte-Carlo energy partitioning model due to Kushner⁵ to relate the specific pump power to the primary ionization and excitation reactions, which ultimately produce the KrF* molecule. For a specific gas mix and electron density, the model calculates the electron energy distribution function. This distribution function, when convolved with energy-dependent excitation or ionization cross sections, yields the W-value (the energy investment in the plasma required to produce a single excitation or ionization event).

KrF Kinetics Model To compute the small-signal gain, absorption, and saturation intensity as a function of gas mix, pressure, and pump power, a time-dependent kinetics model⁶ is used. It solves the coupled set of approximately 70 non-linear reaction equations for the 22 molecular species as a function of time. For this exercise, the values of gain, absorption, and saturation intensity were taken at approximately 100 ns into a constant pump pulse.

Figure 5 shows the small-signal gain over a range of specific pump powers.

Amplified Spontaneous Emission

The 3-D ASE code⁷ provides a steady-state solution to the problem of energy extraction in KrF amplifiers in the presence of amplified spontaneous emission (ASE). An iterative algorithm is used which considers ASE photon transport throughout the active medium, either by direct paths or by diffuse reflection from the side walls. Specular reflection in the end mirror is also included.

Integration over frequency is performed to account for the non-monochromatic nature of the ASE. A Lorentzian frequency dependence is assumed for the spontaneous and stimulated emission cross sections. In addition to the frequency-dependent gain coefficient, transport of ASE photons through the medium includes a frequency-independent absorption coefficient. A portion of the coefficient is assumed to saturate in a manner identical to the saturation of the gain coefficient. Side-wall reflection is modeled by returning a fraction of all incident photons to the medium with a Lambertian cosine-law angular distribution. Wall to wall transport is also included.

Kinetics of the medium are represented via three parameters: the gain coefficient in the absence of ASE or extracting beam g_0 , the upper state life time as determined by spontaneous emissions and quenching collisions τ_u , and the spontaneous emission life time τ_{sp} .

The 3-D numerical simulation approximates the active medium by an array of cubical cells. Walls are approximated by square area elements. Integrals over frequency are via table look up. Typically, the medium is divided into 2500 cells and iteration is continued until changes in average ASE effects are less than two percent. Increasing the cell count above 2500 has little effect on the results.

Figure 6 shows the ASE over a range of gains. Wall reflectance is assumed to be 20% for diode foils and 2% for other (blackened) surfaces.

Time-dependent Energy Extraction

Laser performance was calculated using a time-dependent, one-dimensional propagation code. The right- and left-moving coherent photon fluxes and the medium gain were considered at approximately 200 discrete points along the propagation dimension in the two double-pass amplifiers.

For this exercise, a train of 10 pulses (0.2 ns FWHM Gaussian) spaced every 5 ns were propagated through the two laser amplifiers. The small-signal gain, gain-to-loss ratio, and saturation intensity for each amplifier were obtained from the kinetics model, consistent with the gas mix, pressure, and pump power.

The ASE flux was treated in an approximate time-dependent manner by using a quadratic formula to relate the volume-averaged ASE flux to the volume-averaged (but time-dependent) gain. This formula was obtained from a least squares fit to a series of calculations made with the 3-D ASE code, in which the input extracting flux and small-signal gain were varied. Typically, the volume-averaged ASE flux was less than 0.4 MW cm^{-2} at the point-design pump rate.

The actual output energies reported in this work were obtained by multiplying the energy in the seventh or eighth beam in the train by 24 (the number of beams in the Mercury Phase I design) and the expected energy transmission factor to target (0.58).

Figure 7 shows predicted energy to target over a range of diode current densities at 550 kV diode voltage. The case for a constant, fixed gain-to-loss ratio of 10 is shown, as well as the case for a ratio calculated from the kinetics code. The larger g_0/α from the kinetics code leads to higher energies, particularly at high pump powers. ASE limits performance. The short-pulse extraction of the amplifier prevents effective suppression of the ASE by the laser beams.

Predicted Performance

Diode performance is transformed into specific pump power by reference to a set of electron-beam energy-deposition curves. The average specific pump power over the extracted volume was calculated as a function of electron energy. The diode voltage and current curves yield the temporally resolved specific pump power, when current losses to the hibachi are included.

Predicted pump powers are shown in Figures 8 and 9 for 40% and 60% hibachi transmission. 40% transmission is expected, but 60% curves are presented for comparison, to show the effect of achieving enhanced hibachi transmission.

The energy extraction curves of Figure 7 were used to translate the pump-power Y-axis of Figures 8 and 9 (left side) into predicted energy on target (right side). Figure 8 shows the expected energy delivered to target (above 150 J) with g_0/α derived from the kinetics code. Figure 9 shows delivered energy (above 100 J) for a fixed, constant $g_0/\alpha = 10$. Rapid saturation of the absorption coefficient α is responsible for the higher energy predictions of Figure 8.

Summary

An integrated package of modeling codes has been applied to the design of the final amplifier for Mercury. The predicted performance of the pulsed-power system is translated into specific pump power through an electron energy deposition code. A laser kinetics code translates the pump power into gain, absorption, and saturation intensity. ASE levels are predicted for these calculated laser parameters and specific laser geometry. The time-dependent energy extraction code predicts energy on target in the presence of ASE.

Given conservative parameters - a demonstrated 40% hibachi transmission and a fixed $g_0/\alpha = 10$ - this exercise predicts approximately 140 joules on target, which is above the 100-joule goal of Phase I.

Acknowledgements

This work was performed under the auspices of the United States Department of Energy. The authors are grateful for the extensive ASE modeling performed by W. T. Leland.

References

- 1 L. A. Rosocha, J. A. Hanlon, J. McLeod, M. Kang, B. L. Kortegaard, M. D. Burrows and P. S. Bowling, "Aurora Multikilojoule KrF Laser System Prototype for Inertial Confinement Fusion," Fusion Technology, **11**, 497 (1987).
- 2 J. E. Jones, S. J. Czuchlewski, T. P. Turner, R. G. Watt, S. J. Thomas, D. A. Netz, C. R. Tallman, J. M. Mack and J. F. Figueira, "Performance of the Aurora KrF ICF Laser System," International Conference on Lasers '89, New Orleans, LA, Dec., 1989.

- 3 M. E. Jones and V. A. Thomas, "Three-dimensional Particle-in-cell Modeling of Relativistic Electron Beam Production and Transport for KrF Laser Pumping," LA-UR-90-2170, Beams '90 VIII International Conference on High-power Particle Beams, Novosibirsk, USSR, July, 1990.
- 4 J. C. Comly, W. T. Leland, C. J. Elliott, A. M. Hunter and M. J. Kircher, "Discharge and Kinetics Modeling in Electron-Beam Controlled CO₂ Laser Amplifiers," IEEE J. Quantum Electron. QE17, 1786 (1981).
- 5 M. Kushner, "Energy Partitioning in Rare Gas/Fluorine Gas Mixtures," in Inertial Confinement Fusion at Los Alamos, Progress since 1985, Vol II, Chap II-B, LA-UR-89-265, Sept. 1989, D. C. Cartwright editor.
- 6 S. J. Czuchlewski, D. E. Hanson, B. J. Krohn, A. R. Larson and E. T. Salesky, "KrF Laser Model," in Inertial Confinement Fusion at Los Alamos, Progress since 1985, Vol II, Chap IV-B, LA-UR-89-265, Sept. 1989, D. C. Cartwright editor.
- 7 W. T. Leland, "Amplified Spontaneous Emission in KrF Amplifiers," in Inertial Confinement Fusion at Los Alamos, Progress since 1985, Vol II, Chap V-B, LA-UR-89-265, Sept. 1989, D. C. Cartwright editor.

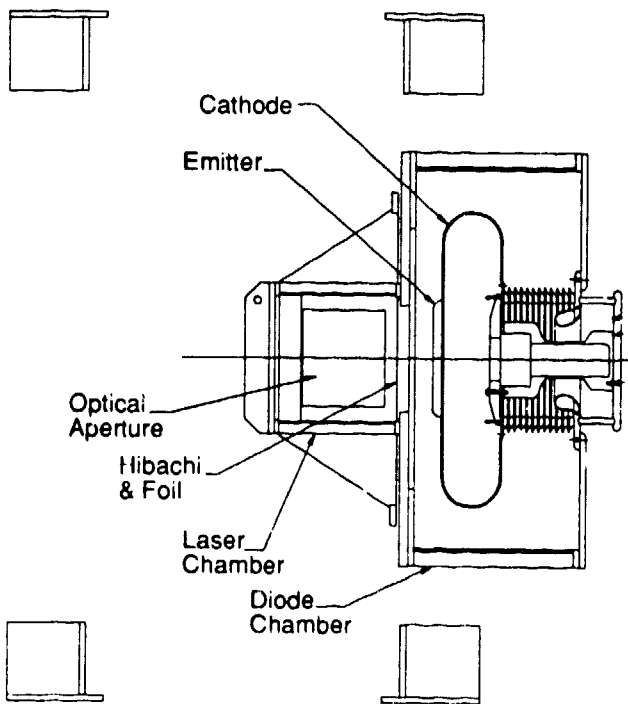


Figure 1: The Mercury final amplifier is a modification of the Aurora Large Aperture Module (LAM).

Final Amplifier Diode Operation

5-cm A-K gap, 1.1 MV Marx charge

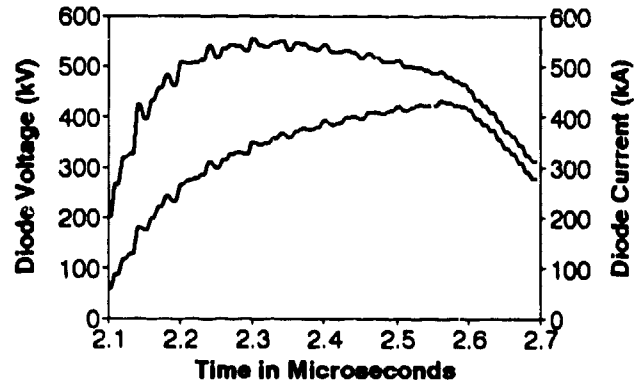


Figure 3: The final amplifier operates in the 500-kV range. Diode closure produces a rising current and falling voltage. Diode power is fairly constant, however.

Circuit Schematic for Final Amplifier Pulsed Power

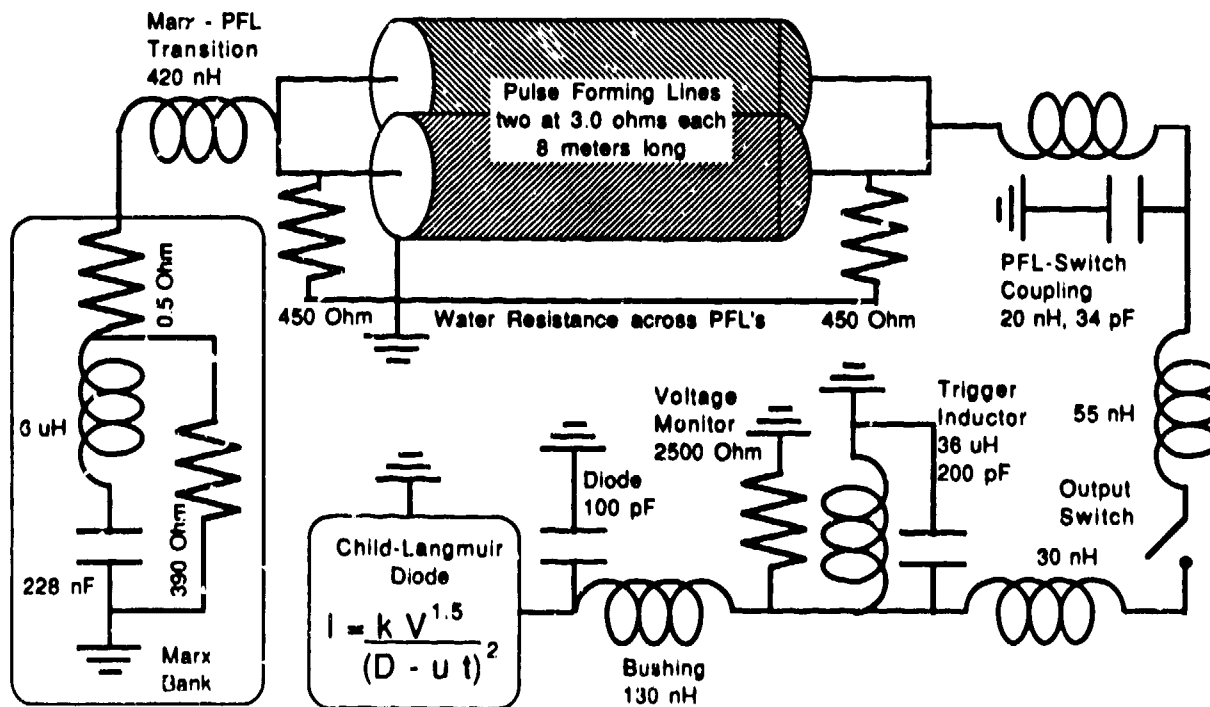


Figure 2: The pulsed-power model for the Mercury final amplifier incorporates shortened LAM pulse-forming lines and a smaller emitter area. The diode model is Child-Langmuir with closure velocity u .

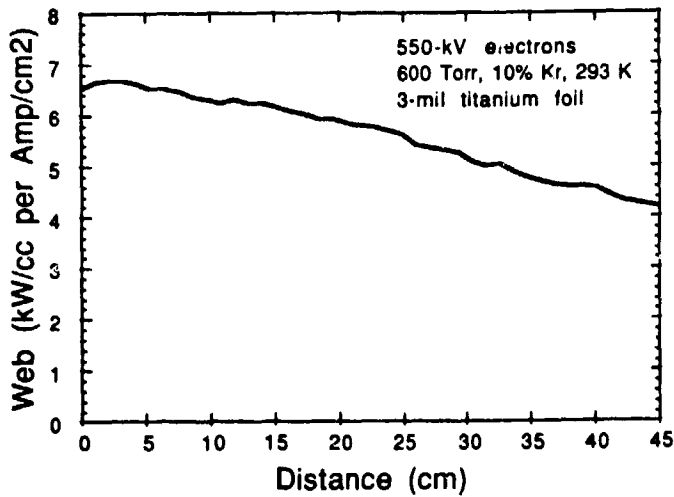


Figure 4: Results of the Electron-beam Energy Deposition code show the specific energy deposition in the laser gas. The unit current density is that delivered from the diode, through the hibachi, to the foil. Deposition falls off with distance from the single diode.

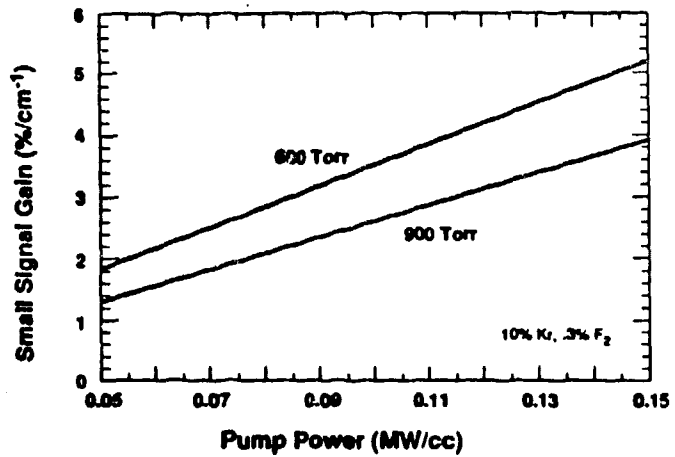


Figure 5: Results of the KrF Kinetics code show the small-signal gain as a function of pump power. Higher collision rates at 900 Torr reduce the gain from the 600 Torr case. The final amplifier will operate at 600 Torr.

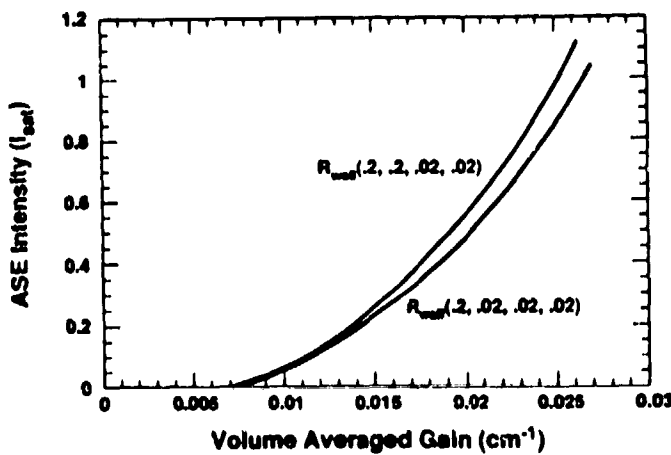


Figure 6: Results of the Amplified Spontaneous Emission code show a rapid increase of ASE with gain. Both the ASE and extracting laser pulse reduce the gain below the small-signal-gain level.

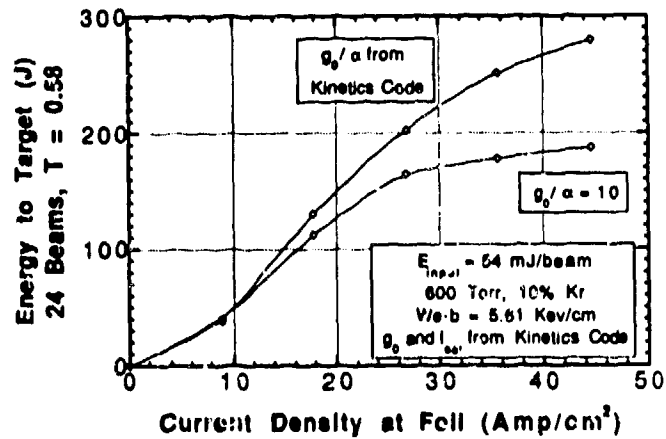


Figure 7: Results of the Time-Dependent Energy Extraction code show the energy delivered to target as a function of pumping levels. The current densities quoted are at the foil (through the hibachi). Energy performance is sensitive to the gain-to-loss ratio at high pumping levels.

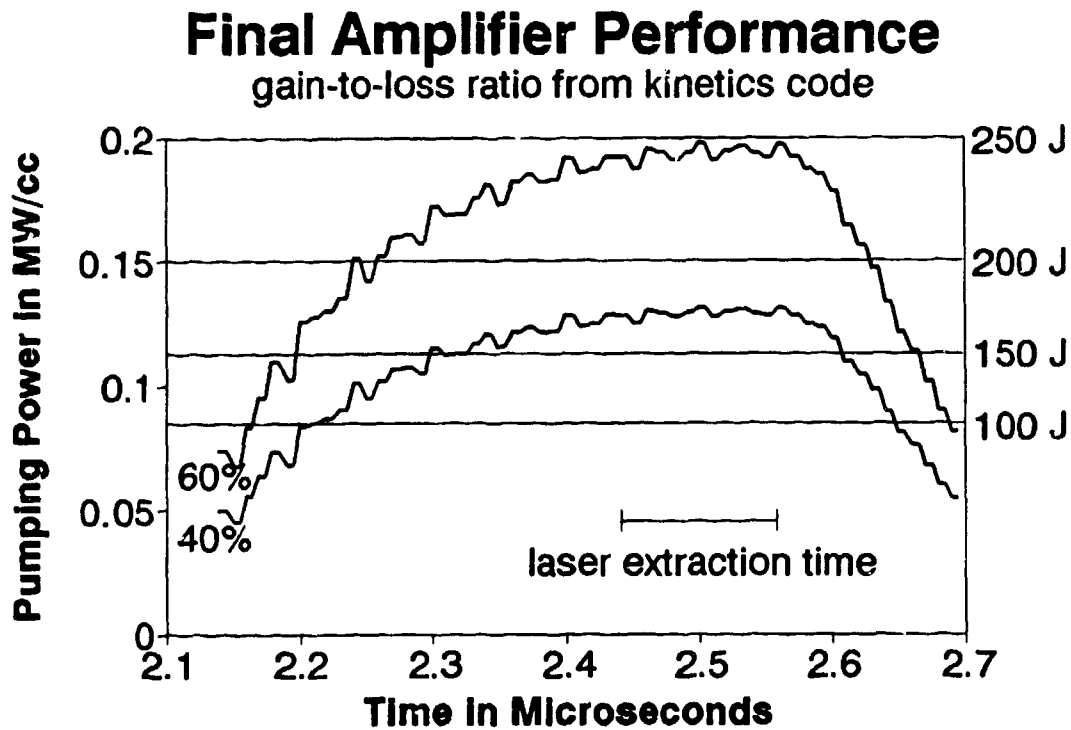


Figure 8: The combined models - Pulsed Power, Electron Energy Deposition, KrF Laser Kinetics, Amplified Spontaneous Emission, and Time-dependent Energy Extraction - predict final amplifier performance. Specific pump power is shown as a function of time (left axis). Energy delivered to target is shown for the corresponding constant pump-power level. With gain-to-loss determined by the kinetics code and for 40% hibachi transmission, the delivered energy is in excess of 150 J.

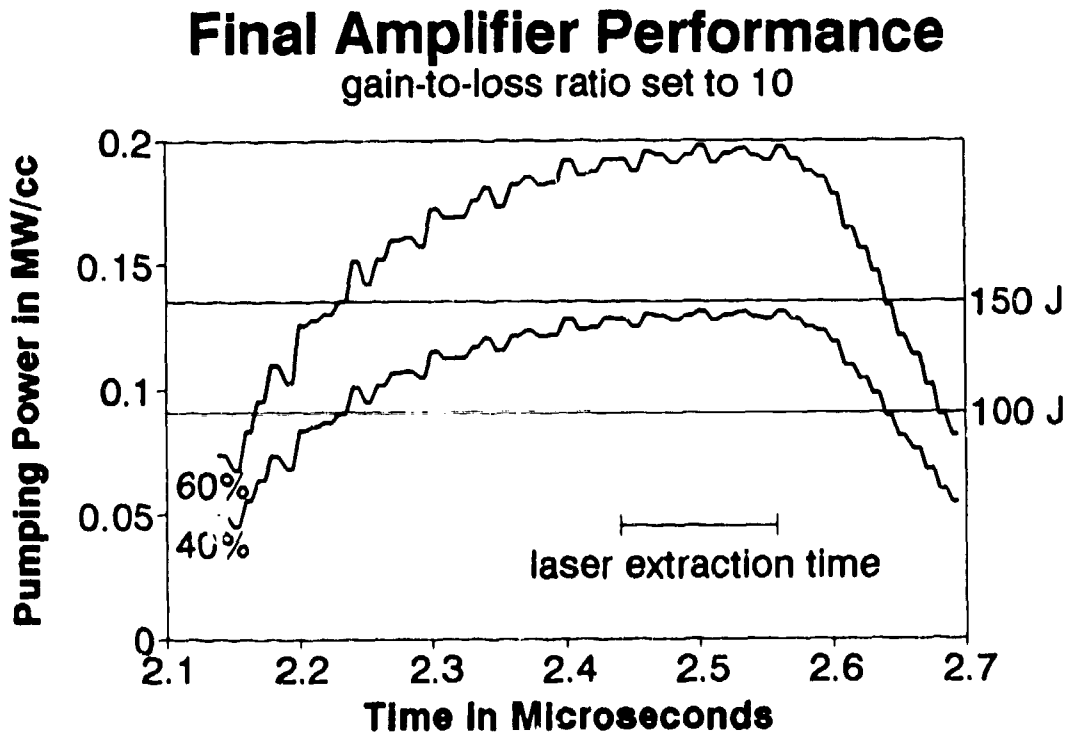


Figure 9: The combined models predict final amplifier performance. With gain-to-loss set at a conservative constant value of 10 and for 40% hibachi transmission, the delivered energy approaches 150 J. This estimate exceeds the 100-J goal of Mercury Phase I.